特集 Cooling Loss Reduction of Highly Dispersed Spray Combustion with Restricted In-Cylinder Swirl and Squish Flow in Diesel Engine*

Masaaki KONO　Masaharu ITO　Masatoshi BASAKI　Takeshi HASHIZUME
Shinobu ISHIYAMA　Kazuhisa INAGAKI

In diesel engines with a straight intake port and a lipless cavity to restrict in-cylinder flow, an injector with numerous small-diameter orifices with a narrow angle can be used to create a highly homogeneous air-fuel mixture that dramatically reduces the NOx and soot without the addition of expensive new devices.

To further improve this new combustion concept, this research focused on cooling losses, which are generally thought to account for 16 to 35% of the total energy of the fuel, and approaches to reducing fuel consumption were explored. First, to clarify the proportions of convective heat transfer and radiation in the cooling losses, Rapid Compression Machine (RCM) was used to measure local heat flux and radiation to the combustion chamber wall. The results showed that though larger amounts of injected fuel increased the proportion of heat losses from radiation, the primary factor in cooling losses is convective heat transfer. Next, 3D simulations were used to predict the cooling loss behavior over the entire combustion chamber, and in conjunction with local heat flux measurements on an actual engine, an analysis was performed to determine where cooling losses are significant and when these cooling losses occur. The results showed that because of the convective heat transfer from the reversed squish flow while the piston is descending, the cooling losses were largest along the side wall of the cavity to the squish region.

Based on the findings above, a piston cavity was designed that suppresses reversed squish flow. The shape of this shallow-dish open-chamber cavity suppressed reversed squish flow including local flow, resulting in reduced fuel consumption.

Key words : Diesel Engine, In-Cylinder Flow, Fuel Consumption, Heat Flux, Radiation

1. INTRODUCTION

Recently, there has been an increasing awareness of environmental and energy problems, which are global in scale. Diesel engines have better fuel consumption than gasoline engines, and there are great hopes for them because they are more flexible in terms of fuel diversification. However, diesel engines have more NOx and smoke than gasoline engines, and thus require expensive fuel injection components and emission control devices to clean these emissions.

Inagaki et al. [1] proposed a new combustion concept that reduces NOx significantly below the Euro6 standard by operating PCCI (Premixed Charge Compression Ignition) in diesel engines that have highly dispersed spray from injectors with numerous small-diameter orifices with a narrow angle combined with low in-cylinder flow. A schematic diagram of an engine for the new combustion concept is shown in **Fig. 1**, and the basic specifications of the engine are shown in **Table 1**. The engine is based on a direct-injection diesel engine found in commercially available vehicles in Europe. A low pressure loop (LPL) EGR system was added to the original engine, which has a conventional high pressure loop (HPL) EGR system. The engine for the new combustion concept is using conventional diesel engine injection components to control costs, and have multi-orifice nozzles with orifices that are smaller than in conventional diesel engines. This type of nozzles with numerous small-diameter orifices can form the highly dispersed spray which can promote the entrainment under the restricted in-cylinder flows. One of an image of the highly dispersed spray is shown in

Table 1　Specifications of engine

Engine type	4-cylinder DI Diesel (2AD-FHV, TOYOTA)
Bore × Stroke (mm)	86 × 96
Displacement (cm³)	2231
Compression ratio	14.0 : 1
Swirl ratio	0.3
Combustion chamber	Lip-less Shallow
Diameter of piston bowl (mm)	φ58
Fuel injection system	Common rail (DENSO)
Discharge coefficient of orifice	0.94
Orifice diameter (mm)	φ0.08
Number of orifice	18
Include angle	140deg.

*Reprinted with permission from SAE paper 2012-01-0689© 2012 SAE International.
Further use or distribution of this material is not permitted without permission from SAE.

Fig. 1. However, this type of nozzles has increased smoke because of the weak penetration of the spray; leading to decreased overall load performance. To resolve this problem, the compression ratio was decreased to 14:1. The low compression ratio makes diffusive combustion phasing advance with early injection timing. This results in lower soot emissions because enough time is created to oxidize soot before the end of combustion. Further, to restore the poor cold startability due to the decreased compression ratio, a straight intake port was adopted to achieve a near-zero swirl ratio. A lipless shallow-cavity (referred to below as the "standard cavity") was also adopted to suppress squish flow. This cavity suppressed convective heat transfer and achieved the required in-cylinder temperature to restore the poor cold startability.

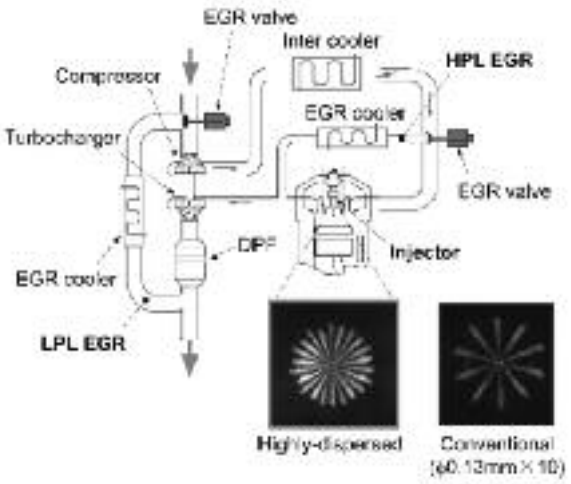

Fig. 1　Schematic diagram of engine and highly-dispersed spray by numerous small-diameter orifices

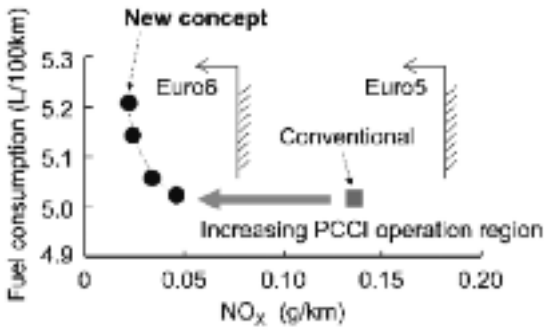

Fig. 2　Trade-off curve between NO_X emission and fuel consumption in equivalent NEDC

Fig. 2 shows a trade-off curve between NO_x emission and fuel consumption in an equivalent New European Driving Cycle (NEDC) [2]. The new combustion concept can offer less than a half of NO_x of Euro6 standard. On the other hand, the new concept increases unburned fuel (HC and CO), which is a characteristic of PCCI combustion; fuel consumption is about the same as conventional diesel combustion. **Fig. 3** shows a comparison of the heat balance between conventional and new combustion concept in the equivalent NEDC [2]. The unburned fuel loss of the new concept is larger than that of conventional diesel combustion. However, the exhaust loss of the new concept is lower than that of conventional diesel combustion, because PCCI combustion can offer a high degree of constant volume energy release, which results in lower exhaust gas temperature. Because the lower gas temperature causes a lower intake pressure which increases the fuel consumption on PCCI combustion [3], the intake pressure is optimized by a variable geometry turbocharger. In addition, the restricted in-cylinder flows can suppress convective heat transfer to the combustion chamber wall; the cooling loss of the new concept is about the same as conventional diesel combustion. As a result, the new combustion concept can achieve low NOx without deteriorating fuel consumption.

Hashizume et al. [4] investigated the mechanism of the emission of unburned fuel and explored ways to decrease fuel consumption by reducing the amount of unburned fuel. The results showed that the primary factor for the emission of unburned fuel during PCCI combustion is incomplete combustion of the combustion chamber space (bulk), and though unburned fuel can be reduced by suppressing the amount of EGR gas, there is an issue with worsened combustion noise. Thus there is a need to develop technologies to decrease fuel consumption working from new perspectives.

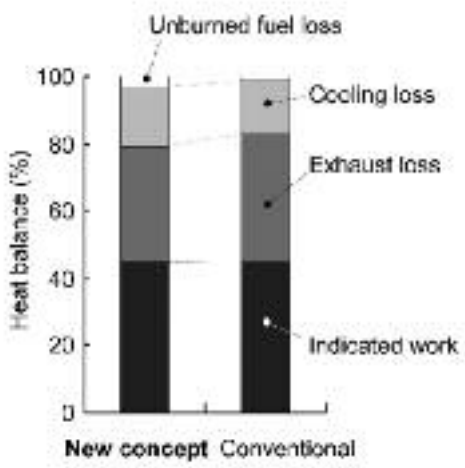

Fig. 3　Heat balance in equivalent NEDC

This research focuses on cooling losses to explore new ways to decrease fuel consumption. Cooling losses are thought to account for 16 to 35% of the total energy of the fuel [5]. As CO_2 restrictions grow more stringent going forward, the development of technologies to reduce cooling losses is necessary [6] to further decrease the fuel consumption of diesel engines. The cooling loss of the new concept still accounts for about 20% and has some leeway to reduce fuel consumption. Generally, combustion in diesel engines is promoted by the mixture of the fuel spray with air through in-cylinder flow, and combustion occurs diffusively. Poor local mixing of fuel and air leads to soot particles and a luminous flame. Because of this, diesel engines have significant radiation from luminous flames, and it is said that the contribution of radiation in cooling losses cannot be ignored. Because of this, the proportion of radiation in cooling losses have been investigated by many researchers, and the estimates vary widely from about 10% [7) 8)] to over 30% [9) 10)]. The combustion in the new concept is combined PCCI with the diffusive diesel combustion at a high load, although it is just PCCI combustion at a low load. Therefore, there is a possibility that radiation is increasing by a luminous flame at a high load.

This research started by using a Rapid Compression Machine (RCM) to analyze the local heat flux and radiation to the combustion chamber wall during this combustion. This revealed the contribution of radiation in cooling losses on the new combustion concept. Next, 3D simulations were carried out in addition to measurements of instantaneous heat flux to the piston wall, cylinder head wall, and cylinder block wall using thin-film thermocouples in order to determine where there are significant cooling losses in the cylinder and when these cooling losses occur. Based on these findings, the cooling loss mechanism resulting from this new combustion concept was observed, and approaches to improving fuel efficiency by decreasing cooling losses were explored.

2. EXPERIMENTAL APPARATUS

In this research, both convective and radiant heat transfer are measured in the RCM, and convective heat transfer is also measured in a test engine, which is same as the engine presented in the introduction section. In addition, 3D simulation is used to predict the cooling loss behavior over the entire combustion chamber.

2.1 Rapid Compression Machine (RCM)

Fig. 4 shows the RCM, which was used to measure local heat flux and radiant heat flux to the combustion chamber wall. A high-temperature, high-pressure atmosphere is created when a cam linked to an air cylinder is rapidly driven using compressed air, and the curved surface of the cam drives the piston, which compresses the in-cylinder air in the combustion chamber and makes it flow [11].

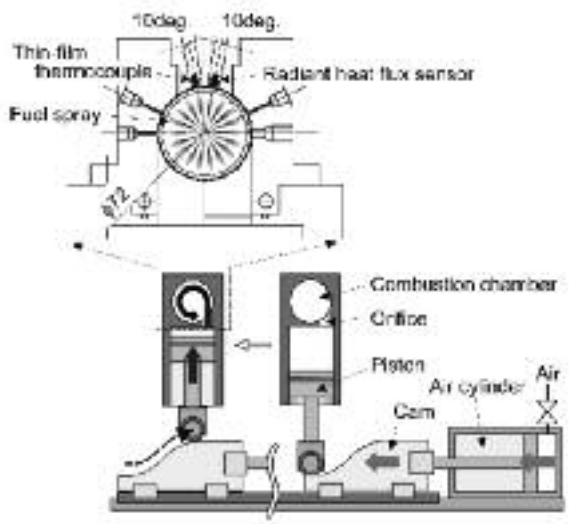

Fig. 4　Schematic diagram of Rapid Compression Machine

The RCM combustion chamber is a cylinder 20mm high with a diameter of 72mm, and differs from an actual engine with cavity. Also, there is no expansion stroke, and the in-cylinder flow behavior differs from that of an actual engine. However, the RCM has a quartz observation window through which the entire combustion chamber can be viewed. The advantage of this is that the combustion behavior can be observed and the local heat flux and radiant heat flux can be measured simultaneously. Because of this, this research used this RCM to analyze the contribution of radiation in cooling losses.

The thin-film thermocouples for measuring the local heat flux and radiant heat flux sensors were installed in the RCM combustion chamber. Though the radiant heat flux is homogenously distributed even if the flame is not homogenously distributed [7], local heat flux depends on the state of the flame, so the effect of the measurement location is significant [12]. Thus in this research, the radiant heat flux sensors were installed where the spray collides with the combustion chamber wall, and the thin-film thermocouples used

to measure local heat flux were installed in bilaterally symmetric locations with respect to the center axis of the spray. Also, a pressure transducer (Kistler 6125B) was installed in the combustion chamber wall to measure the combustion pressure. The signals from the thin-film thermocouples and radiant heat flux sensors are amplified 500 times by the DC amplifier (Kyowa Electronic Instruments DA-510B), and, together with the signal from the pressure transducer, are acquired by the data recorder (Yokogawa Electric DL-1640). In addition to the measurements of local heat flux and radiant heat flux, a high-speed camera (Photron FASTCAM SA1.1) was used to visually record the combustion behavior. The speed of the camera is 20,000fps, and the resolution is 512 x 512 pixels.

2.2　Sensors for measuring heat flux

The local heat flux was measured by thin-film thermocouples employing the method used by Enomoto et al. [13]. The structure of the thin-film thermocouples, which are custom-made, are shown in **Fig. 5**. To decrease the heat capacity and increase the response time of the surface temperature-measuring junction, the junction was formed by sputtering a thin layer of gold between 0.13mm diameter Constantan wire inserted in the center of the sensor to the body of the sensor. The back temperature-measuring junction is formed from 0.13mm diameter Constantan wire and Chromel wire. The directions of heat conduction were taken into consideration before installing the thin-film thermocouples. The local heat flux to the combustion chamber was calculated by setting the surface and back temperature measurements as the boundary conditions and using numerical analysis to find the first-order temperature distribution within the thin-film thermocouple [14]. The thickness of the gold layer is around 5 μm to 7μm, which impacts a response time of the thin-film thermocouple. The measurements of the local heat flux shown below include less than 0.5ms delay in the response. However, no compensation was applied in this research because validation results of the instantaneous heat flux between measurement and 3D simulation were favorable.

The local heat flux obtained from the thin-film thermocouples was made up of the convective heat transfer and radiant heat flux. Thus, radiant heat flux was measured at the same time to determine the contribution of radiation in cooling losses.

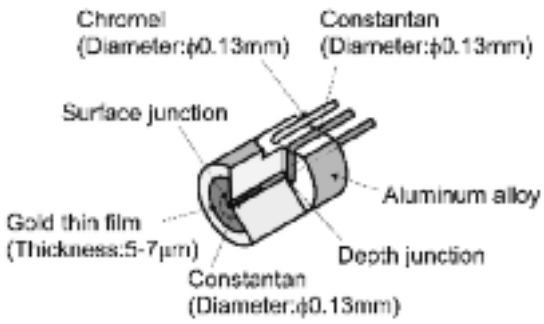

Fig. 5　Thin film thermocouple for heat flux measurement

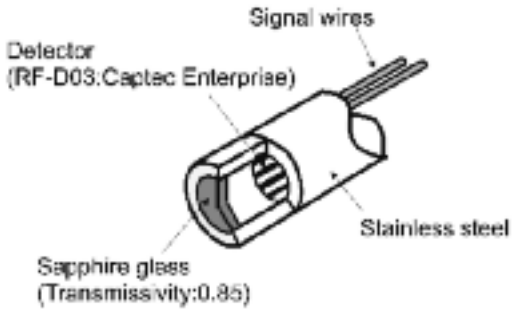

Fig. 6　Radiant heat flux sensor

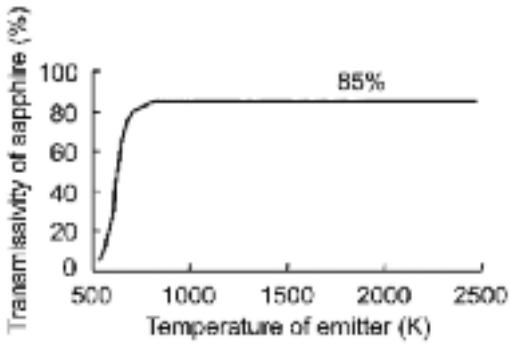

Fig. 7　Relationship between temperature of emitter And transmissivity of sapphire

The structure of the radiant heat flux sensor is shown in **Fig. 6**. The radiant heat flux sensor has a detector (Captec Enterprise RF-D03) comprised of areas with two different emissivity characteristics, and the radiant heat flux is measured based on the temperature difference. A sapphire window was used to protect the detector from the combustion flame, which is the method used by Oguri et al. [15]. The transmissivity of the sapphire window is changing with temperature of an emitter. **Fig. 7** shows the relationship between temperature of an emitter and transmissivity of a sapphire. The sapphire window transmits 85% of the radiant heat flux emitted by the luminous flame. The measurements shown below have been compensated using this value. The

transmissivity of the sapphire decreases less than 800K. It means that the radiation from the wall, whose temperature is 433K, cannot transmit the sapphire window. However, this does not impact the measurement. Because, according to Stefan-Boltzmann law, radiation from luminous flame is much larger than radiation from the chamber wall. In addition, the radiant heat flux sensor's detector has a 60ms delay. Thus the measurements shown below have been compensated using Equation (1).

$$V_{inst} = V_{raw} + C\frac{dV_{raw}}{dt} \qquad (1)$$

V_{inst} is the instantaneous radiant heat flux, V_{raw} is the experimental raw value of the radiant heat flux, and C is the delay of the radiation sensor. The radiant heat flux compensated using Equation (1) was also validated by two color temperature radiometry.

2.3 Engine used to measure heat flux

The test engine used to measure heat flux and the engine presented in the introduction section are entirely same. Thin-film thermocouples were installed on the piston walls, cylinder head walls, and cylinder block wall of the test engine to measure the local heat flux. The measurement locations are shown in **Fig. 8**. Thin-film thermocouples were installed on three locations on the piston: the side wall of the cavity (P1), the radiused portion of the cavity (P2), and the bottom of the cavity (P3). The signal wire from the thin-film thermocouples installed on the piston was guided out of the engine by attaching a link mechanism to the larger end of the connecting rod, making it follow the connecting rod and link, and finally out the engine based on the method by Ando et al. [16]. Thin-film thermocouples were installed on two locations of the cylinder head: the squish region (H1) and the cavity region (H2). Additionally, a pressure transducer (Kistler 6125B) was installed on the cylinder head. The thermocouples on the cylinder block were located at point B1, which is 6mm from the top edge.

The output voltage of the thin-film thermocouples was amplified 500 times by the DC amplifier (Kyowa Electronic Instruments DA-510B), and together with the output from the pressure transducer, was acquired by the recording device (Ono Sokki DS-2000) as 100-cycle average integral data.

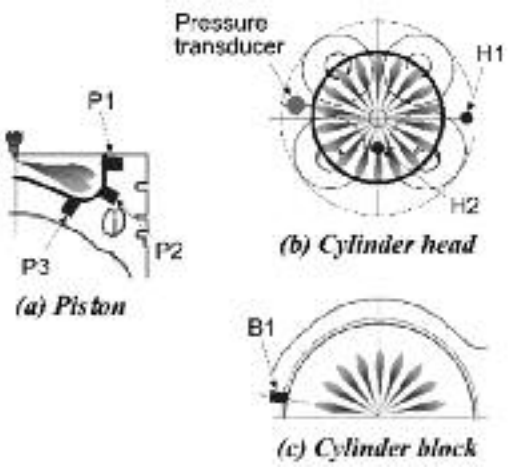

Fig. 8　Locations of heat flux measurement

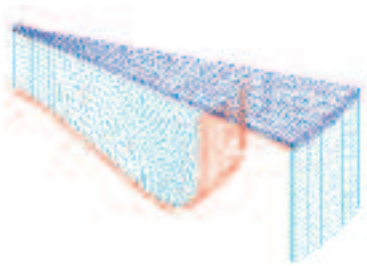

Fig. 9　Perspective view of computational grid at TDC (One-eighteenth sector of the combustion chamber)

Table 2　Configuration of 3D simulation by STAR-CD

Turbulence	Standard k-ε model with improved wall function
Spray	DDM
Droplet breakup	Reitz-Diwakar model
Ignition	Shell model
Combustion	CTC model

2.4 3D simulations

The computational fluid dynamics application STAR-CD (version 3.26) was used to perform the simulation. **Fig. 9** shows the computational grid at TDC. The intake and exhaust valves on the cylinder head wall are not considered. Because of this, the calculation period is from IVC to EVO. The number of meshes at IVC is 15567, and the number of meshes at TDC is 6738. The temperature of the piston wall, cylinder head wall, and cylinder block wall were set using the surface temperatures obtained from the thin-film thermocouples.

Table 2 shows the submodel used. The turbulent flow model is the standard k-ε model [17]. Generally, to analyze

the behavior in the vicinity of the wall boundary with a high degree of precision, it is necessary to make the mesh sufficiently fine at the wall boundary. However, because this results in increased calculation time, this is not practical. For this reason, the gas velocity distribution and temperature distribution in the vicinity of the wall boundary are often approximated with a wall function in order to achieve both improved precision and shortened calculation time. In this research, STAR-CD was provided with an improved wall function that takes into account the change in the thermal properties of the wall boundary due to temperature changes based on the paper by Kleemann et al. [18].

The fuel spray was modeled with the Discrete Droplet Model (DDM). The DDM requires the initial droplet diameter, the initial velocity, as well as the initial spray direction to be defined as the initial conditions. For this simulation, the initial droplet diameter of the spray was set to the orifice diameter of the fuel spray nozzle. The initial velocity and direction of the spray were defined based on the results of the steady-state flow calculations for the inside of the fuel spray nozzle at maximum needle-lift. This is why the initial velocity of the spray was assumed to be proportional to the instantaneous injection rate. The physical properties of the fuel spray were set to n-$C_{12}H_{26}$, which is similar in composition to diesel. The Reitz-Diwaker model [19] was used to model droplet breakup. The constants of the model were adjusted so that the spray penetration at ordinary temperature and high density matches the experimental results. The ignition model and combustion model were the Shell model and the CTC (Characteristic Time-scale Combustion) model [20] respectively. The model constants were adjusted so that the ignition timing and rate of heat release matched those in an actual engine.

3. RESULTS AND OBSERVATIONS

3.1 Contribution of radiation in cooling losses

The RCM was used to measure the local heat flux and the radiant heat flux to the combustion chamber to analyze the proportions of convective heat transfer and radiation in cooling losses, and the results are described in this section.

The experimental conditions are shown in **Table 3**. The temperature and pressure reflect the injection timing for PCCI combustion. **Fig. 10** shows the results from the high-speed camera as well as the local heat flux, radiant heat flux, and apparent rate of heat release. The injection volume was 40mm^3/st, assumed a high load operation. Because the combustion occurs diffusively in such a large amount of injection, a luminous flame is occurring from the center of the combustion chamber to the wall surface area. Despite the large luminous flame, the radiant heat flux is small compared to the total local heat flux. The total local heat flux and radiant heat flux during the period of heat release were integrated to analyze the proportion of radiation in cooling losses. The results are shown in **Fig. 11**. The horizontal axis shows injection volume. Though the proportion of radiation increases as the injection volume is increased, the proportion of radiation in cooling losses was 8% when the injection volume was 40mm^3/st.

It is assumed that the soot emission from the combustion process with the highly dispersed spray is lower than that with the conventional spray, because this type of nozzle with small-diameter orifices can promote spray atomization and entrainment. Consequently, though the influence of

Table 3　Experimental conditions

Injection pressure (MPa)	60
Injection timing	Compression end
Atmosphere	Air
Ambient pressure (MPa)	2.6
Ambient temperature (K)	750
Wall temperature (K)	433

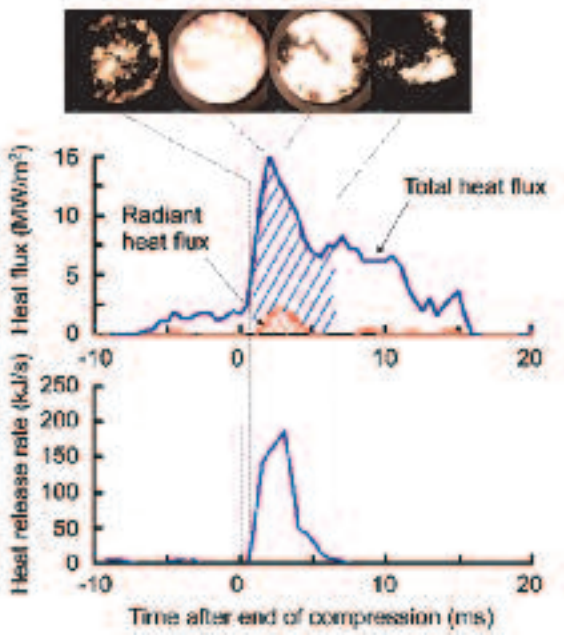

Fig. 10　Combustion behavior, heat flux and apparent rate of heat release (Injection quantity:40mm^3/st)

radiation in cooling losses increases as injection volume is increased, it was found that the primary factor in cooling losses is convective heat transfer.

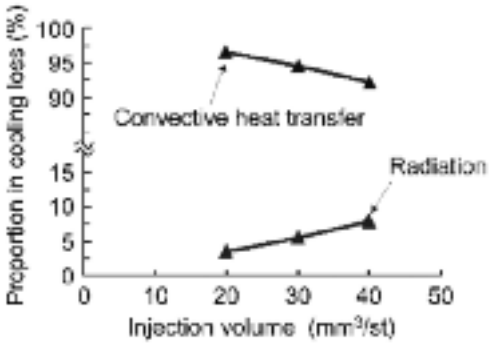

Fig. 11　Proportion of Radiation and Convective heat transfer in total cooling loss

3.2　Where and when cooling losses occur

3D simulations were used to predict the cooling loss behavior over the entire combustion chamber, and the findings were verified with actual engine measurements; the results are shown in this section. As shown in **Table 4**, the engine tests were performed at 2100r/min under a high load operation.

Table 4　Experimental conditions

Engine speed (r/min)	2100
IMEP (kPa)	1080
Brake torque (Nm)	128
Injection pressure (MPa)	130
Total injection volume (mm³/st)	38
Pilot injection timing (deg. BTDC)	59, 35
Main injection timing (deg. BTDC)	10
Intake pressure (kPa)	170
Intake temperature (K)	313

Fig. 12 shows the results of a 3D simulation of the in-cylinder gas temperature and the heat flux to the combustion chamber wall. Based on the in-cylinder gas temperature distribution, high-temperature combustion gas can be seen rotating over the area spanning the radiused portion of the cavity to the bottom of the cavity with the descending piston; in addition, flow from inside the cavity to the squish region can be seen. It can be seen from the heat flux to the combustion chamber wall, the side wall of the cavity is where heat flux is predominant. As the piston descends, the heat flux to the squish region also increases. On the other hand, the bottom of the cavity and cylinder block wall sees almost no heat flux.

The results of the heat flux simulation shown in **Fig. 12** were integrated separately over one cycle for the piston wall, cylinder head wall, and cylinder block wall, and the breakdown of the cooling losses was calculated with respect to the total energy of the fuel injected in one cycle. The results are shown in **Fig. 13**. Most cooling losses take place through the piston wall. Based on these results, it is believed that with this type of combustion, there will be large cooling losses in the area from the side wall of the cavity to the squish region while the piston is descending.

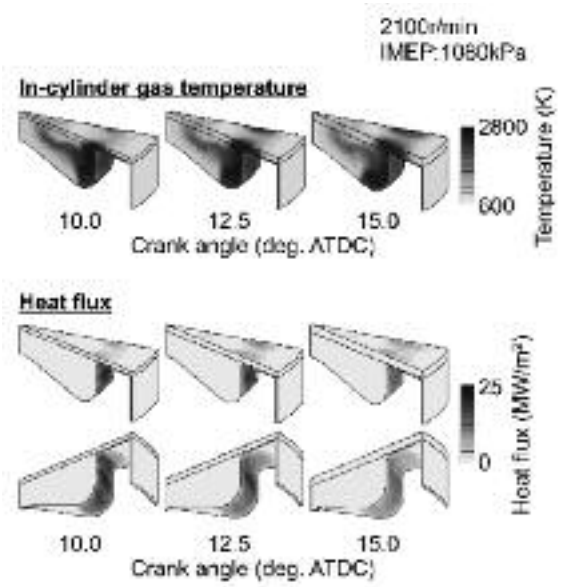

Fig. 12　Distribution of in-cylinder gas temperature and heat flux simulated by STAR-CD

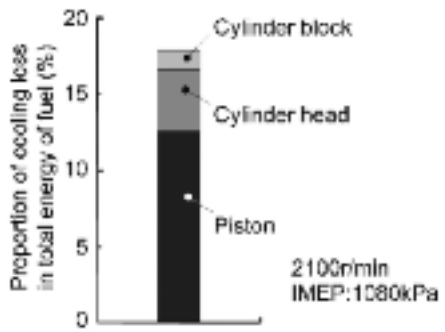

Fig. 13　Proportion of cooling loss in total energy of fuel simulated by STAR-CD

The results of the 3D simulation were verified using measurements from an actual engine. The results of this verification are shown in the next figure. **Fig. 14** shows a comparison of the in-cylinder pressure, rate of heat release and

instantaneous heat flux obtained from the simulation with those measured during the engine tests. The in-cylinder pressure, ignition timing, rate of heat release and instantaneous heat flux match the results obtained from the engine tests.

Fig. 15 shows a comparison of the local cooling losses obtained from the simulation with those measured during the engine tests. Even with the measurements made during the engine tests, the cooling losses through the piston wall were greater than those to the cylinder head wall and cylinder block wall. In particular, cooling losses to the side wall of the cavity were predominant. Consequently, it is believed that the results of simulation were in accordance with the measurements of the actual engine.

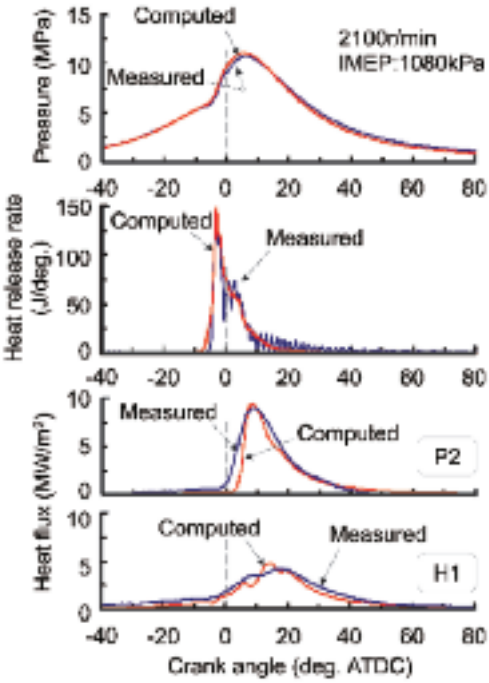

Fig. 14　Comparison of pressure profile, apparent rate of heat release and local heat flux between experiment and simulation

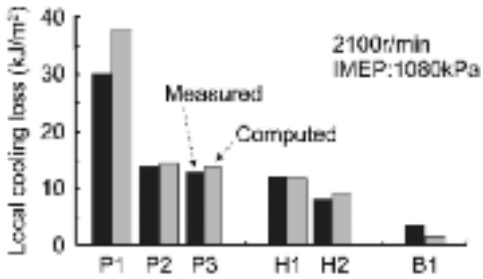

Fig. 15　Comparison of local cooling loss between experiment and simulation

Fig. 16 shows the measurements of instantaneous heat flux through the combustion chamber wall. During the period of ignition and combustion, the heat flux to the radiused portion of the cavity (P2) and the bottom of the cavity (P3) increased. Afterwards, the heat flux to the side wall of the cavity (P1) and the squish region (H1) increases during the descent of the piston.

Based on the results of the 3D simulation and heat flux measurements, the primary location cooling loss occurs is along the side wall of the piston cavity to the squish region while the piston is descending.

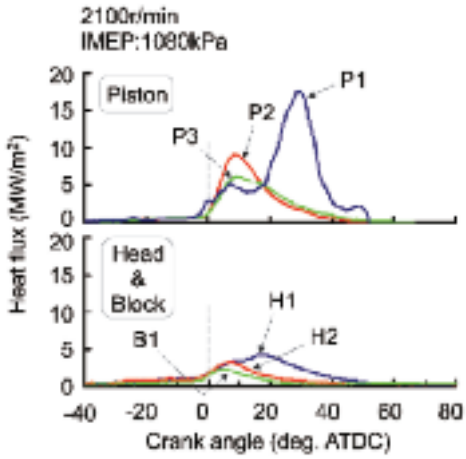

Fig. 16　Heat flux measured by thin film thermocouples

3.3　Approaches to decrease fuel consumption

The cooling loss of the new combustion concept still accounts for about 20%, and is thought that it has some leeway to reduce fuel consumption. As indicated above, the 3D simulations and actual engine measurements show that the area along the side wall of the cavity to the squish region is where the most cooling losses occur, and the cooling losses occur during the descent of the piston. This section explores the approaches that should be taken to reduce cooling losses based on the findings above.

Fig. 17 shows the simulation results for in-cylinder gas velocity and in-cylinder gas temperature distribution during the descent of the piston. The in-cylinder gas flow can be seen as the spray and combustion rotating at the bottom of the cavity, as well as the reversed squish flow into the squish region that can be seen moving along the side wall of the cavity. It is thought that with this reversed squish flow, high temperature gas flows along the side wall of the cavity to the squish region, causing cooling losses through convec-

tive heat transfer. In order to reduce the convective heat transfer, ways of suppressing reversed squish flow during the descent of the piston were explored.

Generally, under a certain compression ratio, the following can be done to suppress squish flow during the reciprocating motion of the piston.

1. Make the cavity a shallow dish, in order to reduce the volume of the squish region.
2. Widen the distance between the piston and cylinder head at TDC, in order to increase the cross-sectional area from the cavity to the squish region.

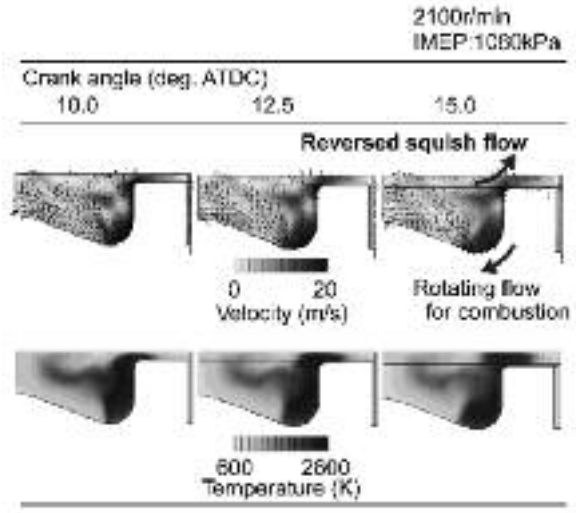

Fig. 17　Distribution of in-cylinder gas velocity and temperature simulated by STAR-CD

The in-cylinder gas velocity distribution with the cavity shapes that were devised based on this approach are shown in **Fig. 18** when the crank angle is 10deg ATDC during motoring. In Case 1, a shallow-dish cavity results in improved suppression of reversed squish flow velocity, but the suppression of gas flow velocity in local regions in the vicinity of the side wall of the cavity is insufficient. In Case 2, the distance between the piston and squish region at TDC has been widened, and the cross-sectional area of the opening from the cavity to the squish region has been increased; though improved suppression of gas velocity near the side wall of the cavity can be seen, local areas with high gas velocity can be seen close to the squish region of the cylinder head. In Case 3, however, the cross-sectional area of the opening from the cavity to the squish region is changed gradually for a tapered cavity; this results in improved suppression of reversed squish flow including local gas velocity in the vicinity of the squish region from the side wall of the cavity to the cylinder. The cavity shape used in Case 3 referred to as a "tapered shallow-dish cavity"; the reduced cooling losses and decreased fuel consumption were confirmed and the results are described below.

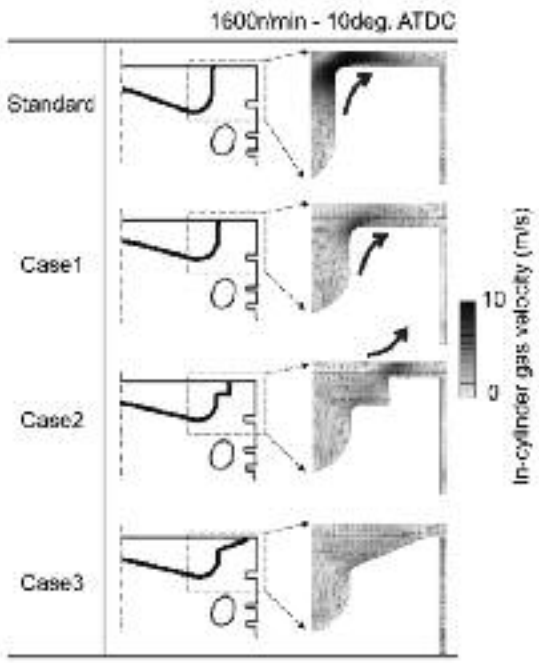

Fig. 18　Shape of piston bowl and distribution of in-cylinder gas velocity simulated by STAR-CD

3.4　Confirming the improvement in fuel consumption

The reduced cooling losses and improved fuel consumption were confirmed for the tapered shallow-dish cavity, and the results are described in this section.

Fig. 19 shows the results of the 3D simulation of the in-cylinder gas temperature and the heat flux to the combustion chamber wall at 15deg. ATDC, comparing the standard cavity and the tapered shallow-dish cavity. Although the reversed squish flow is suppressed by the tapered shallow-dish cavity, a high temperature region in the tapered shallow-dish cavity can be seen at the squish region; it seems like the same combustion phasing in the standard cavity. It is thought that spray penetration can promote the mixing of air and fuel spray in the tapered shallow-dish cavity. However, because of suppressing the reversed squish flow, the heat flux from the side wall of the cavity to the squish region can be decreased in the tapered shallow-dish cavity.

Simulations were performed comparing the standard cavity and the tapered shallow-dish cavity, and the heat flux was integrated over one cycle separately for the piston wall, cylinder head wall, and cylinder block wall in order to cal-

culate the breakdown of cooling losses. The results are shown in **Fig. 20**. As expected, for the tapered shallow-dish cavity, the improved suppression of cooling losses through the piston wall and the cylinder wall were seen.

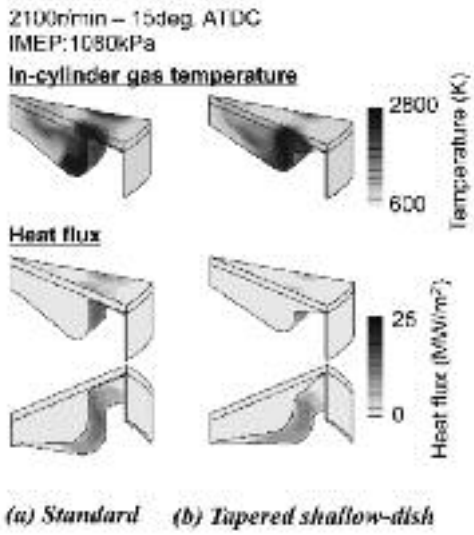

Fig. 19　Distribution of in-cylinder gas temperature and heat flux simulated by STAR-CD

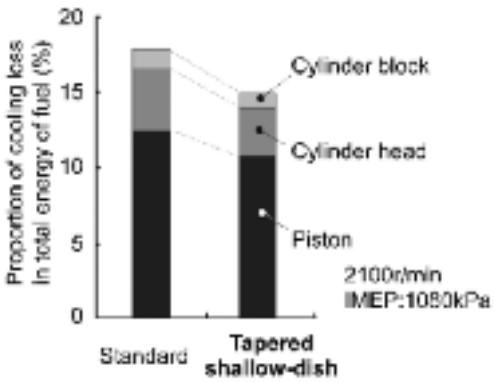

Fig. 20　Proportion of cooling loss in total heat value simulated by STAR-CD

A tapered shallow-dish with the same design as the modeled one was manufactured and installed in the test engine. **Fig. 21** shows the instantaneous heat flux to the squish region (H1) of the cylinder head. The rate of heat release of the tapered shallow-dish cavity was as same as that of the standard cavity. As expected, the heat flux of the tapered shallow-dish cavity was suppressed during the descent of the piston.

Fig. 22 shows the relationship between IMEP and the heat balance of a standard cavity and a tapered shallow-dish cavity. The heat balance calculated in **Fig. 22** was based on the experimental results; measured in-cylinder pressure and the exhausted unburned fuel (HC and CO). The increase in IMEP here was not done by changing the injection pressure, pilot injection timing, pilot injection amount or main injection timing; only the main injection amount was increased. As IMEP is increased, cooling losses and exhaust losses increase. However, the suppression of cooling losses can be seen in the tapered shallow-dish cavity compared to the standard cavity. As IMEP is larger, the injection amount is also larger. As a result, it is assumed that the combustion region spreads to the squish region outside the cavity. However, compared to the standard cavity, the tapered shallow-dish cavity suppresses reversed squish flow while the piston is descending, resulting in suppression of convective heat transfer along the side wall of the cavity to the squish region. It is believed that because of this, even with the overall heat balance, the tapered shallow-dish cavity results in suppression of cooling losses.

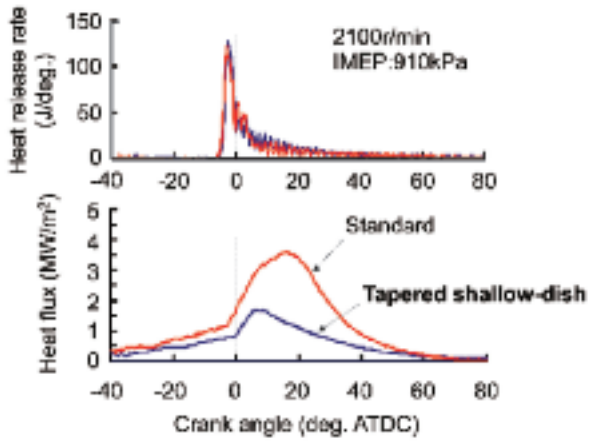

Fig. 21　Comparison of apparent rate of heat release and heat flux at squish region (H1) between Standard and Tapered shallow-dish cavity

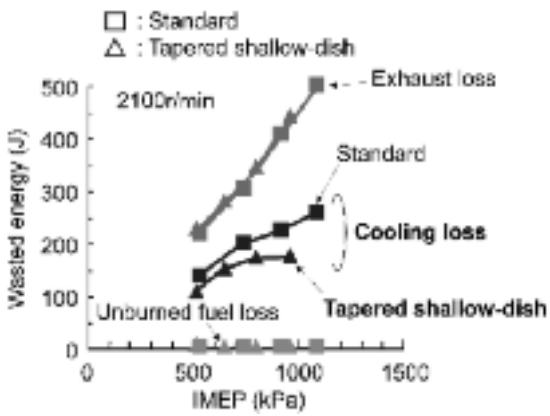

Fig. 22　Relationship between IMEP and heat value

Fig. 23 shows the relationship between IMEP and ISFC with the tapered shallow-dish cavity compared to the standard cavity. It can be seen that the tapered shallow-dish cavity results in reducing cooling losses compared to the standard cavity, resulting in improved fuel consumption.

In general, the restricted in-cylinder flows suppress the entrainment of a spray; the soot emission increases. However, the tapered shallow-dish cavity can retain the entrainment because the spray penetration of the highly dispersed spray is distributed in the entire combustion chamber. As a result, the soot emission remains low in the new concept. In addition, the NOx emission also remains low because the highly dispersed spray decreases an area of a high temperature region. **Fig. 24** shows the relationship between NOx emission and fuel economy in the equivalent NEDC. The fuel economy in the equivalent NEDC is assumed based on **Fig. 23**. It can be seen that the tapered shallow-dish can decrease the fuel economy without deteriorating the emissions (NOx and soot).

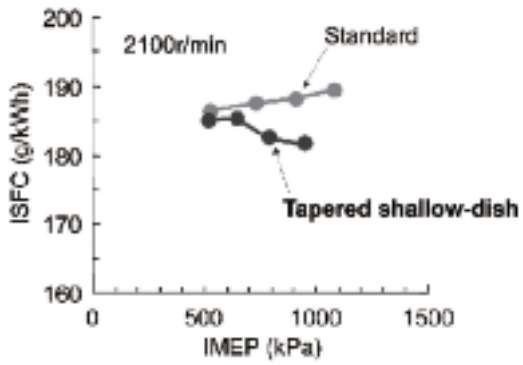

Fig. 23　Relationship between IMEP and ISFC

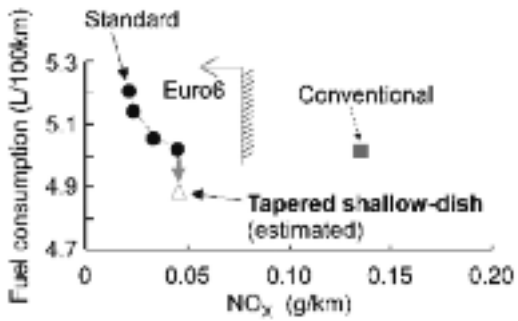

Fig. 24　Trade-off curve between NOx emission and fuel consumption in equivalent NEDC

4. Summary

PCCI using an injector with numerous small-diameter orifices was recreated using an RCM, and the contribution of radiation in cooling losses was clarified.

Using actual engine measurements and 3D simulations, the local heat flux to the piston wall, cylinder head wall, and cylinder block wall was determined in a diesel engine with a highly dispersed spray achieved with an injector with numerous small-diameter orifices with a narrow angle, in addition to low in-cylinder flow; the primary locations where cooling losses occur and when these losses occur were determined.

Based on the results obtained, the mechanism of cooling losses was observed, and approaches to improving fuel consumption through improved cooling losses were explored from the perspective of cavity shape.

1. The primary factor of cooling losses is convective heat transfer. Although the proportion of radiation in cooling losses increases as the injection amount is increased, at an injection amount of 40mm^3/st, this proportion is 8%.
2. With this type of combustion, the locations where cooling losses occur the most are along the side walls of the piston cavity to the squish region. The heat flux is the greatest when the piston is descending.
3. While the piston is descending, the convective heat transfer arising from the reversed squish flow from inside the cavity to the squish region results in cooling losses.
4. The tapered shallow-dish cavity, which gradually changes the cross-sectional area of the opening from the cavity to the squish region, suppresses reversed squish flow along the side wall of the cavity to the squish region, including local gas flow.
5. Compared to a standard cavity, the tapered shallow-dish cavity has decreased cooling losses, which results in decreased fuel consumption.

References

1) Inagaki, K., Mizuta, J., Fuyuto, T., Hashizume, T. et al., SAE Int. J. Engines 4(1):2065-2079, 2011, doi:10.4271/2011-01-1393.

2) Hashizume, T. Ito, H. Inagaki, K. and Kuzuyama, H., Proceedings of the 21st Internal Combustion Engine Symposium (Japan),

pp.503-508, 2010 (in Japanese)
3) Lee, S., Gonzalez, D., M., and Reitz, R., SAE Technical Paper 2007-01-0121, 2007, doi:10.4271/2007-01-0121
4) Hashizume, T. Kawae, T. Kuzuyama, H. Kono, M. Inagaki, K. and Tomoda, T., Transactions of Society of Automotive Engineers of Japan, Vol. 42, No.2, pp.439-444, 2011 (in Japanese)
5) Heywood, J. B. “ Internal Combustion Engine Fundamentals”, McGraw-Hill, Inc., p.674, 1988
6) Furuno, S. and Tomoda, T., Journal of the Combustion Society of Japan, Vol.51, No.155, pp.23-30, 2009 (in Japanese)
7) Kuboyama, T. Kosaka, H. and Aizawa, T., Transactions of the Japan Society of Mechanical Engineers, Series B, Vol.74, No.741, pp.1191-1198, 2008 (in Japanese)
8) Yoshikawa, T. and Reitz, R., Journal of Thermal Science and Technology, Vol.4, No.1, pp.86-97, 2009
9) Ebersole, G., Myers, P., and Uyehara, O., SAE Technical Paper 630148, 1963, doi:10.4271/630148.
10) Borman, G. L. and Nishiwaki, K., Progress in Energy and Combustion Science, Vol.13, pp.1-46, 1987
11) Yamashita, H. Basaki, M. Ogawa, T. and Nishida, K., Proceedings of the 48th Symposium (Japanese) on Combustion, pp.230-231, 2010 (in Japanese)
12) Emi, M. Suzuki, Y. Katsuramaki, T. Sugihara, T. Shimano, K. and Enomoto, Y., Transactions of Society of Automotive Engineers of Japan, Vol. 40, No.2, pp.355-360, 2009 (in Japanese)
13) Enomoto, Y. and Furuhama, S., Transactions of the Japan Society of Mechanical Engineers, Series B, Vol.50, No.453, pp.1353-1362, 1984 (in Japanese)
14) Enomoto, Y. Ohya, T. Ishii, M. Enomoto, K. and Kitahara, N., Transactions of the Japan Society of Mechanical Engineers, Series B, Vol.57, No.539, pp.2421-2427, 1991 (in Japanese)
15) Oguri, T. and Inaba, S., “Radiant Heat Transfer in Diesel Engines,” SAE Technical Paper 720023, 1972, doi:10.4271/720023.
16) Ando, A. Kosuda, T. Sawada, T. and Mitani, S., Proceedings of JSAE Annual Congress, No.26-07, pp.1-4, 2007 (in Japanese)
17) Kong, S., Han, Z., and Reitz, R., SAE Technical Paper 950278, 1995, doi:10.4271/950278.
18) Kleemann, A. P. Gosman, A. D. and Binder, K. B., The 5th International Symposium on Diagnostics and Modeding of Combustion in Internal Combustion Engines (COMODIA), pp.123-131, 2001
19) Reitz, R. and Diwakar, R., SAE Technical Paper 860469, 1986, doi:10.4271/860469.
20) Kong, S., Han, Z., and Reitz, R., SAE Technical Paper 950278, 1995, doi:10.4271/950278.

＜著　者＞

河野　正顕
（こうの　まさあき）
総研　研究1部　博士（工学）
エンジン内燃焼システムの解析に従事

馬﨑　政俊
（ばさき　まさとし）
パワトレインシステム開発部
パワトレイン全般に関わる研究・開発テーマの企画に従事

伊藤　昌晴
（いとう　まさはる）
総研　研究1部
ディーゼル噴霧・燃焼システムの開発に従事

橋詰　　剛
（はしづめ　たけし）
トヨタ自動車株式会社　エンジン先行制御システム開発部
博士（工学）
高効率低排気を実現するディーゼル燃焼システムの開発に従事

石山　　忍
（いしやま　しのぶ）
トヨタ自動車株式会社
エンジン先行制御システム開発部
高効率低排気を実現するディーゼル燃焼システムの開発に従事

稲垣　和久
（いながき　かずひさ）
株式会社 豊田中央研究所
機械1部燃焼研究室
将来ディーゼル燃焼系の開発に従事